MATERIALS CHEMISTRY FRONTIERS

CHINESE CHEMICAL SOCIETY

ROYAL SOCIETY OF CHEMISTRY

RESEARCH ARTICLE

View Article Online
View Journal | View Issue

Cite this: *Mater. Chem. Front.*, 2021, **5**, 7824

Rational design of D–π–D hole-transporting materials for efficient perovskite solar cells†

Yang Mei Ou, Lin Xie, * Tai Wu, Rong Jun Zhao, Peng Wang, Yuan Ju Zhao, Gao Yuan Liu, Qian Lai, Li Qiong Zhu and Yong Hua *

Received 15th July 2021,
Accepted 7th September 2021

DOI: 10.1039/d1qm01015h

rsc.li/frontiers-materials

Organic–inorganic halide perovskites (OIHPs) are nature-abundant raw materials with prospects as a low-cost renewable energy source encouraged by the solution-processed capability of OIHPs. However, the application of an expensive hole-transporting material (HTM), such as 2,2′,7,7′-tetrakis (*N*,*N*-di-*p*-methoxyphenyl-amine)-9,9′-spirobifluoren (Spiro-OMeTAD), in the most efficient OIHP solar cells limits their commercialization at a large scale. Here, a series of D–π–D hole-transporting materials are designed and synthesized from inexpensive starting materials with high yield *via* simple synthetic routes for application in OIHP solar cells. It is found that strengthening the conjugation by inserting a conjugated bridge of (3,7-di(thiophen-2-yl)dibenzo[*b*,*d*]thiophene) (QY3) in the synthetic molecule, leads to a higher hole mobility and deeper HOMO level, resulting in an increased fill factor, improved open-circuit voltage and increased power conversion efficiency of 19.28%, which is comparable to that of OIHP solar cells based on Spiro-OMeTAD (19.30%). The results show that QY3-HTM could be a promising candidate for low-cost OIHP solar cells. The present work provides a guideline for rational design *via* prudent control of the core units of the hole transport materials for application in low-cost OIHP solar cells.

1. Introduction

Within the last decade, substantial progress has been made in the field of organic–inorganic hybrid perovskite (OIHP) solar cells due to their impressive power conversion efficiency (PCE), competitive low fabrication cost and ease of processing.[1–4] Ever since the pioneering work by Park reporting the first solid-state OIHP solar cells based on a conventional structure (*n*–*i*–*p*) with a PCE of 9.7% in 2011,[5] much research attention has been focused on controlling the perovskite composition,[6,7] morphology,[8,9] and hole and electron transport layers (HTLs and ETLs).[10–13] Comprehensive improvements in all these areas have resulted in the current PCE record of 25.6%.[14] This rapid progress is very encouraging for the future commercialization of OIHP solar cells. State-of-the art HTL materials are an essential part of OIHP solar cells, and are responsible for extracting/transporting the holes at the perovskite/hole-transporting material (HTM) interface and preventing moisture penetration, leading to enhancement in the performance and stability of the OIHP solar cells. To date, the small molecule 2,2′,7,7′-tetrakis (*N*,*N*-di-*p*-methoxyphenyl-amine)-9,9′-spirobifluoren (named Spiro-OMeTAD) is the most representative HTL in high-performance OIHP solar cells. Unfortunately, the tedious synthesis with low yield and time-consuming purification of Spiro-OMeTAD seriously hinder its potential in large-scale industrial applications of OIHP solar cells[15]. Therefore, it is highly desirable to develop cost-effective synthetic strategies and efficient alternatives to Spiro-OMeTAD to achieve high PCE and long-term stability of OIHP devices. This has stimulated great research efforts aimed at developing various types of HTMs by means of facile synthetic routes, such as small molecules,[15,16] polymers[17,18] and inorganic HTMs.[19,20] In comparison to polymeric and inorganic HTMs, small-molecule-based HTMs hold the advantages of well-defined chemical structure, facile synthetic route and handy batch-to-batch reproduction[21]. Recently, small-molecule-based HTMs with a D–π–D structure, where D indicates an electron-donating group and π is a conjugated bridge, have been studied extensively due to their outstanding hole-transporting capability through their strong intermolecular π–π stacking interaction in solid-state thin films.[22–25] Moreover, the hole-transporting properties and molecular interaction of D–π–D-based HTMs could be rationally modified in accordance with the π-conjugation within the synthetic molecules. However, systematic studies on the selection of small-molecule-based HTMs with optimal conjugated bridge for efficient hole extraction and transportation are still lacking.

Yunnan Key Laboratory for Micro/Nano Materials & Technology, School of Materials and Energy, Yunnan University, Kunming 650091, China. E-mail: l.xie@ynu.edu.cn, huayong@ynu.edu.cn

† Electronic supplementary information (ESI) available. See DOI: 10.1039/d1qm01015h

In this work, we present three novel D–π–D-based HTMs employing 9*H*-fluorene, dibenzo[*b*,*d*]thiophene and 3,7-di(thiophen-2-yl)dibenzo[*b*,*d*]thiophene π bridges as the center core units, linked with electron-donating groups of diphenylamine for highly efficient OIHP devices (abbreviated as QY1, QY2, and QY3). It is noted that all the HTMs investigated are synthesized from relatively inexpensive raw materials with high yields. Through prudent control over the core units of the π bridge, the hole-transporting performance of D–π–D-based HTMs can be effectively managed *via* a well-established π-conjugated bridge. Our systematic study demonstrates the influence of the π-conjugated bridge on the optoelectronic and hole transport properties, and highlights the importance of the π-conjugated bridge in enhancing the related performance of OIHP solar cells. We find that the D–π–D-based HTM with QY3 shows better hole mobility than its counterparts, and is even comparable to the conventional Spiro-OMeTAD. As a result, our findings not only offer a facile and low-cost D–π–D-based HTM for efficient OIHP solar cells, but also rationalize the design of highly efficient and stable D–π–D-based HTMs for OIHP solar cell applications in the future.

2. Experimental

2.1 Synthetic routes

The synthetic routes of QY1, QY2 and QY3 are described in the ESI.†

2.2 Device fabrication

The fluorine-doped tin oxide (FTO) substrates were etched with zinc powder and HCl acid (concentration 4 M) to form the desired electrode pattern. The substrates were cleaned in an ultrasonic bath for half an hour in the following order: deionized water, acetone and ethanol. A compact layer of TiO_2, intended to block the recombination current at the FTO support, was prepared on cleaned FTO substrate by spray pyrolysis of solution (0.2 M titanium isopropoxide and 2 M acetylacetone in isopropanol). Afterwards, a layer of mesoporous TiO_2 particles were spin-coated on the FTO glass with a thickness of 200 nm. The perovskite films were deposited from a precursor solution containing formamidinium iodide (FAI) (1 M), PbI_2 (1.1 M), methylammonium bromide (MABr) (0.2 M) and $PbBr_2$ (0.2 M) in anhydrous DMF : DMSO = 4 : 1 (v/v). The perovskite solution was spin-coated in a two-step program: first at 1000 r.p.m. for 10 s and then at 5000 r.p.m. for 30 s. During the second step, 120 μL of chlorobenzene were poured onto the spinning substrate 12 s before the end of the program. The substrates were then annealed at 100 °C for 1 h in a nitrogen-filled glove box. Here, the QY1, QY2, QY3 and Spiro-OMeTAD/chlorobenzene solutions were prepared with addition of 9.05 μL lithium bis(trifluoromethanesulfonyl)imide (Li-TFSI), 520 mg Li-TFSI in 1 mL acetonitrile, 15.80 μL *tert*-butylpyridine (tBP) and 3.92 μL FK209 (300 mg FK209 in 1 mL acetonitrile). As a last step 80 nm of gold top electrode were thermally evaporated under high vacuum.

2.3 Characterizations

Current–voltage characteristics were measured under 100 mW cm^{-2} (AM 1.5G illumination) using a Newport solar simulator (model 91160) and a Keithley 2400 sourcemeter. A certified reference solar cell (Fraunhofer ISE) was used to calibrate the light source for an intensity of 100 mW cm^{-2}. Incident photon-to-current conversion efficiency (IPCE) spectra were recorded using a computer-controlled setup consisting of a Xenon light source (Spectral Products ASB-XE-175), a monochromator (Spectra Products CM110), and a potentiostat (Lab Jack U6 DAQ board), calibrated by a certified reference solar cell (Fraunhofer ISE). Electron lifetime measurements were performed using a white LED (Luxeon Star 1 W) as the light source. The photocurrent decay was determined by monitoring photocurrent transients by applying a small square-wave modulation to the base light intensity. The voltage scan rate was 10 mV s^{-1} and no device preconditioning, such as light soaking or forward voltage bias applied for a long time, was applied before starting the measurement. The cells were masked with a black metal mask limiting the active area to 0.0625 cm^2 and reducing the influence of the scattered light. ^1H NMR spectra were recorded using a Bruker Ultrashield 400 Plus NMR spectrometer. High-resolution matrix-assisted laser desorption/ionization time-of-flight (MALDI-TOF) mass spectra were obtained with a Bruker Autoflex MALDI-TOF mass spectrometer. ^{13}C NMR spectra were recorded on a VNMRS 600 (Agilent, USA) spectrophotometer. The cross-sectional scanning electron microscopy (SEM) image of the device was characterized by an FEI Nova NanoSEM 450. Atomic force microscopy (AFM) images were collected in air on a scanning probe microscope (Being Nano-Instruments, Ltd, CSPM5500) using a tapping mode. Photoluminescence (PL) and time-resolved PL (TRPL) spectra were recorded on an FLS 1000 fluorescence spectrometer. Contact-angle measurements were conducted by a JC20002D1.

3. Results and discussion

3.1 Optical and electrochemical properties

To investigate the influence of the D–π–D-based HTMs on device performance, we fabricated solar cell devices with QY1-, QY2- and QY3-based OIHP films on a planar device architecture of FTO/compact titanium dioxide (cp-TiO_2)/mesopores TiO_2 (mp-TiO_2)/$(FAPbI_3)_{0.85}(MAPbBr_3)_{0.15}$/HTLs/Au (Fig. 1(a)). The molecular structures of QY1, QY2 and QY3 are shown in Fig. 1(b). For comparison, we intentionally inserted a sulfur atom with a lone pair of electrons in QY2 to enhance the conjugation of QY1 without changing the π-bridge conjugation length. To gain further insight into the effect of π-conjugated bridge length on the resulting OIHP solar cells, we extended the length of the π-bridge conjugation (see QY3) by inserting two thiophene groups based on QY2. The detailed synthetic routes are described in Scheme S1 (ESI†). The synthetic cost of the QY-HTMs are listed in Tables S1–S5 (ESI†).

The maximum absorption peaks (λ_{max}) of QY1, QY2, QY3 and Spiro-OMeTAD are 364 nm, 371 nm, 427 nm and 384 nm,

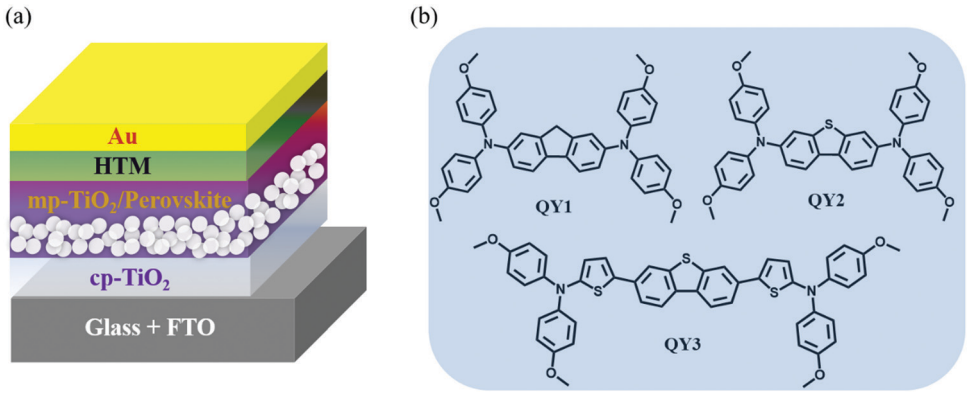

Fig. 1 (a) Schematic illustration of conventional planar OIHP solar cells. (b) Chemical structures of the studied molecules QY1, QY2 and QY3, respectively.

respectively, as shown in Fig. 2(a). The gradual red shift of the λ_{max} is attributed to extending the π-conjugation in the central scaffold by inserting the sulfur atom and the longer π-bridge, which has proven to favour the intramolecular charge transfer.[26] Additionally, all of the QY-HTMs show weak absorption capacities in the visible region, implying that the HTLs would not compete with the perovskite film for light absorption in OIHP solar cells. A similar red shift tendency for the photoluminescence (PL) peaks of QY1 (λ_{max} = 424 nm), QY2 (λ_{max} = 440 nm), QY3 (λ_{max} = 505 nm) and Spiro-OMeTAD (λ_{max} = 433 nm) are observed, as shown in Fig. 2(b), which is consistent with the results of UV-visible absorption. The optical band gaps (E_g) of QY1, QY2, QY3 and Spiro-OMeTAD were estimated to be 3.05 eV, 3.00 eV, 2.63 eV and 2.98 eV, respectively, as determined from the intersection of the normalized UV-visible absorption and PL spectra. The highest occupied molecular orbital (HOMO) energy levels of QY1 (−5.10 eV), QY2 (−5.11 eV), QY3 (−5.12 eV) and Spiro-OMeTAD (5.09 eV) were determined from the differential pulse voltammetry results, as shown in Fig. 2(c).[27] The lowest unoccupied molecular orbital (LUMO) energy levels of QY1 (−2.05 eV), QY2 (−2.11 eV), QY3 (−2.94 eV) and Spiro-OMeTAD (−2.11 eV) were calculated

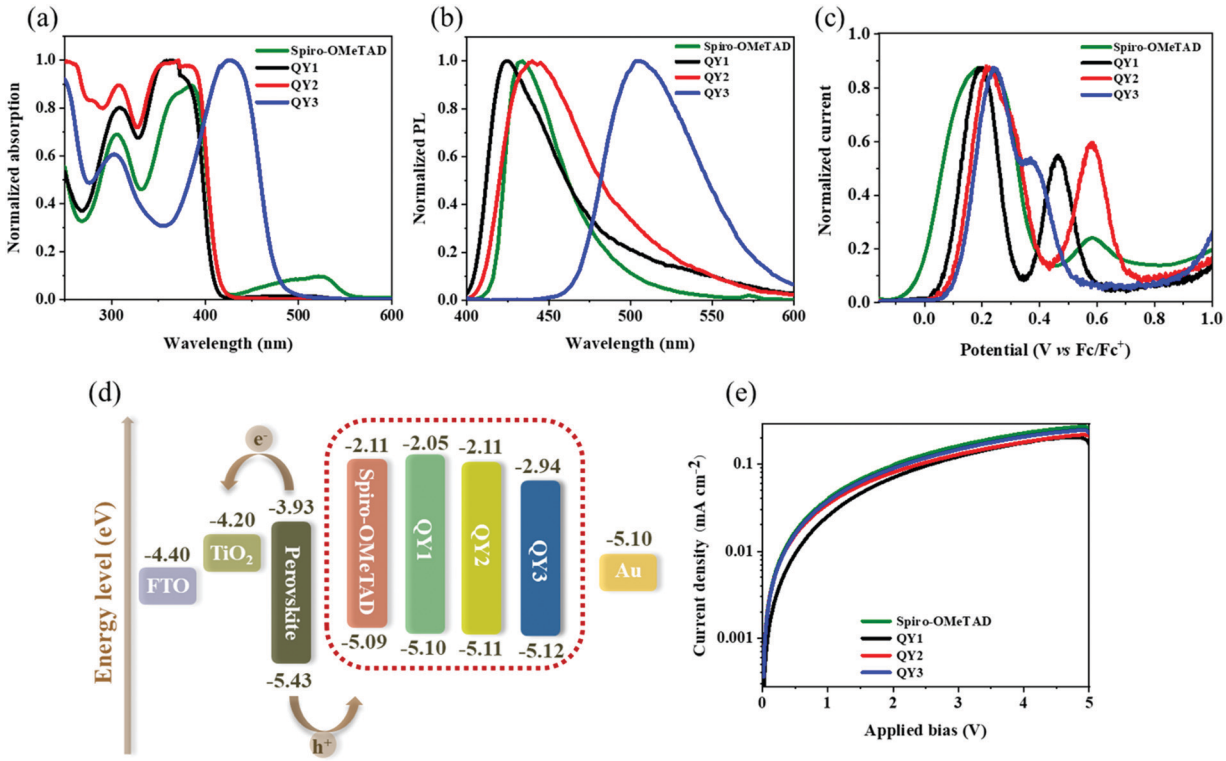

Fig. 2 (a) Normalized UV-visible absorption spectra of Spiro-OMeTAD, QY1, QY2 and QY3 in CH_2Cl_2 solution. (b) Normalized PL spectra of Spiro-OMeTAD, QY1, QY2 and QY3 in CH_2Cl_2 solution. (c) Normalized differential pulse voltammetry results of Spiro-OMeTAD, QY1, QY2 and QY3. (d) Energy level diagram of individual layers used in OIHP solar cells. (e) *J*–*V* curves obtained from hole-only FTO/PEDOT:PSS/HTLs/Au devices.

Table 1 Photophysical and electrochemical data for QY1, QY2, QY3 and Spiro-OMeTAD

HTM	λ_{max} [a] (nm)	λ_{onset} [b] (nm)	E_{HOMO} [c] (eV)	E_{LUMO} [d] (eV)	E_g [e] (eV)	Hole mobility [f] ($cm^2\ V^{-1}\ s^{-1}$)
QY1	364	406	−5.10	2.05	3.05	1.10×10^{-4}
QY2	371	412	−5.11	2.11	3.00	1.98×10^{-4}
QY3	427	471	−5.12	2.94	2.63	2.13×10^{-4}
Spiro-OMeTAD	384	415	−5.09	2.11	2.98	2.18×10^{-4}

[a] Measured in CH_2Cl_2 solution. [b] Calculated from the intersection of the normalized absorption and emission spectra measured in CH_2Cl_2 solution. [c] Using cyclic voltammetry in CH_2Cl_2 solution, $E^{Fc}_{1/2}$= 0.2 eV, $E_{HOMO} = -5.1 - (E_{1/2} - E^{Fc}_{1/2})$. [d] $E_{LUMO} = E_{HOMO} + E_g$. [e] $E_g = 1240/\lambda_{onset}$. [f] Hole mobility of HTMs.

from the formula of $E_{LUMO} = E_{HOMO} + E_g$[28]. The calculated band diagram of the different components in OIHP devices and the corresponding photophysical and electrochemical data for QY1, QY2 and QY3 are displayed in Fig. 2(d) and summarized in Table 1. We found that a deeper HOMO level is obtained as we enhance the conjugation in the core center, from QY1 to QY3. The deeper HOMO energy level in QY3 can be assigned to the insertion of a conjugated π-bridge into the backbone of QY3.[29] All the HOMO levels of QY-HTMs are well aligned at the interface of perovskite/Au. In addition, the LUMO values of the HTLs fulfil the requirement of preventing electron backflow from the perovskite film to the counter electrodes. To investigate the influence of the various π-conjugations on the hole mobility, a space-charge-limited current analysis *via* the hole-only device was performed (Fig. 2(e)). The hole mobilities of QY-HTMs and Spiro-OMeTAD were evaluated using the Mott–Gurney equation $J = \frac{9}{8}\varepsilon_0\varepsilon_r\mu\frac{V^2}{d^3}$, where J is the current density, ε_o is the vacuum permittivity (8.85×10^{-12} F m^{-1}), ε_r is the dielectric constant of the material (organic film usually takes the value 3), μ is the hole mobility, V is the applied bias, and d is the film thickness, respectively.[30,31] Compared to the hole mobility of QY1 (1.10×10^{-4} $cm^2\ V^{-1}\ s^{-1}$) and QY2 (1.98×10^{-4} $cm^2\ V^{-1}\ s^{-1}$), QY3 exhibits a higher hole mobility of 2.13×10^{-4} $cm^2\ V^{-1}\ s^{-1}$, demonstrating that strengthening the π-conjugation in the core center for D–π–D-based HTMs can efficiently increase the hole mobility and promote hole transportation. This implies that the high mobility would allow QY3 to be a potential alternative to Spiro-OMeTAD.

3.2 Surface morphology

We also characterized the morphology of QY-HTMs over the OIHP films using AFM and SEM. The top view AFM and SEM images shown in Fig. 3 and clearly show that all the QY-HTL-treated OIHP films produce full coverage and pin-hole-free capping layers over the perovskite films. The surface roughness of the OIHP film is greatly reduced, from 16.9 nm to 12.9 nm, 12.1 nm and 10.7 nm when QY1, QY2 and QY3 were applied, respectively. The results indicate that QY3 shows a more uniform OIHP film than QY2 and QY1, which would be able to contribute to the hole transport in the device, and stability.

3.3 Device performance

Fig. 4(a) presents the current density–voltage (J–V) curves of the Spiro-OMeTAD- and QY-HTM-modified OIHP devices measured under standard AM 1.5G illumination in ambient conditions, and the corresponding photovoltaic parameters are summarized in Table 2. The best QY1-modified OIHP devices display PCE, open-circuit voltage (V_{oc}), current density (J_{sc}) and fill factor (FF) values of 18.23%, 1.09 V, 22.54 mA cm^{-2} and 73.79%, respectively. QY2-modified OIHP devices show an increased FF and V_{oc}, resulting in an increased PCE of 18.52%. Meanwhile, devices modified with QY3 show further improvement in FF and V_{oc}, with the champion device exhibiting a PCE of 19.28%, which is comparable to the performance of devices modified with Spiro-OMeTAD. The IPCE spectra of

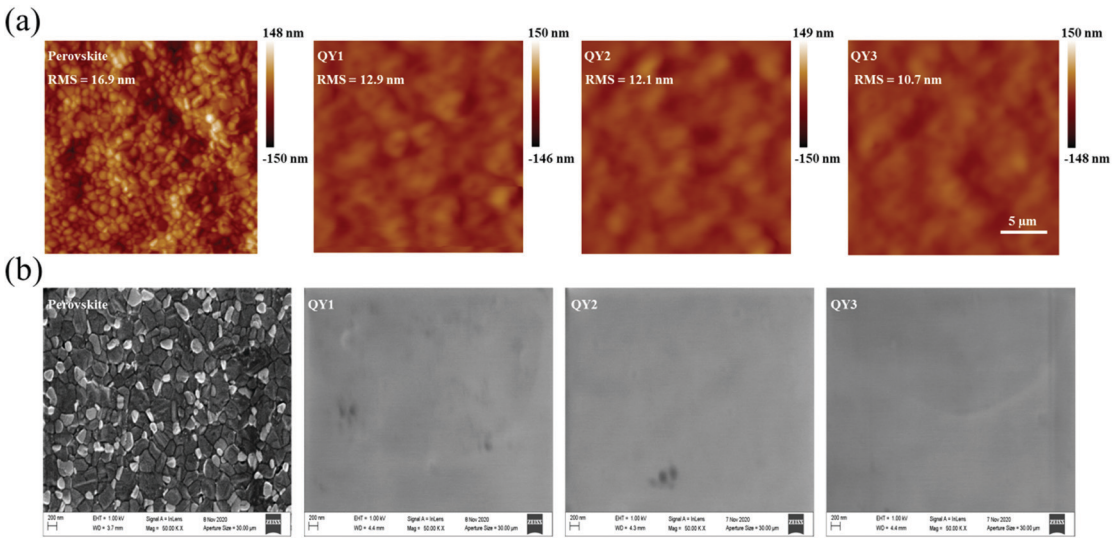

Fig. 3 (a) AFM images of pristine perovskite, QY1, QY2 and QY3 films. (b) SEM images of pristine perovskite, QY1, QY2 and QY3 films prepared on FTO substrates.

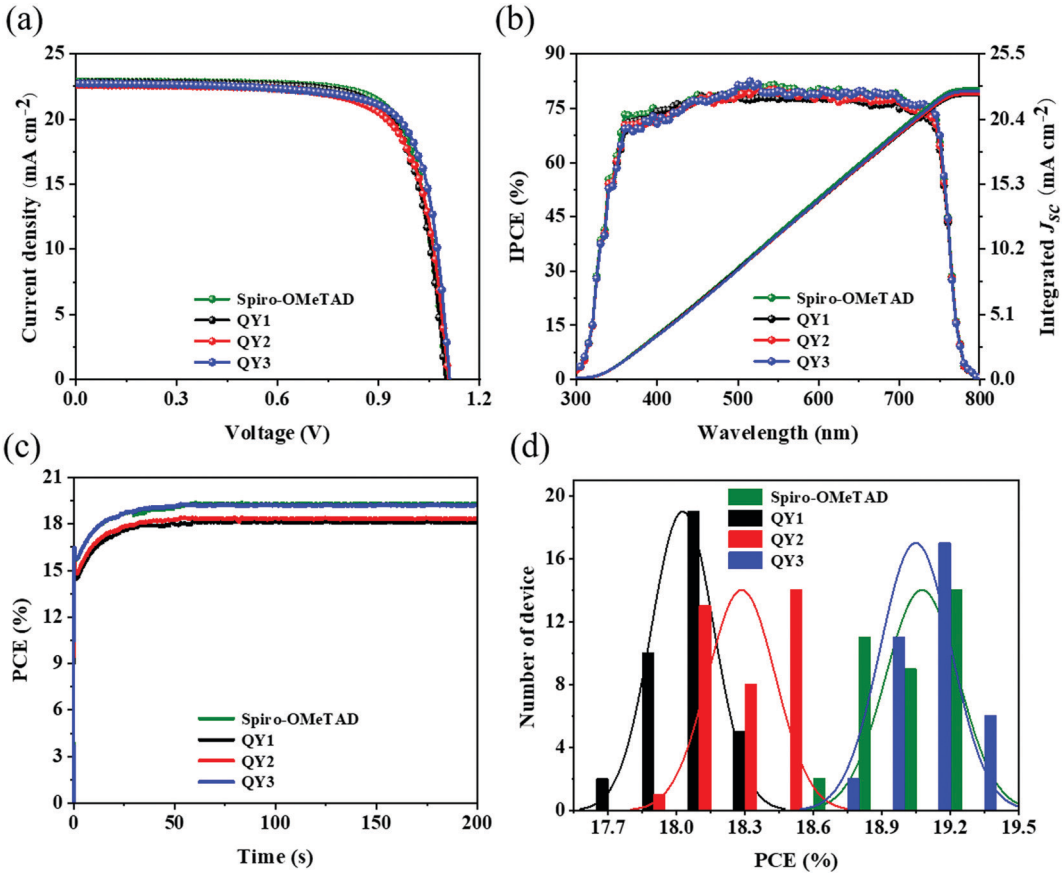

Fig. 4 (a) *J–V* curves (reverse scan) for OIHP solar cells fabricated with QY-HTLs and Spiro-OMeTAD. (b) IPCE spectra and the integrated short-circuit current density (J_{sc}) of the QY-HTL- and Spiro-OMeTAD-modified OIHP solar cells. (c) Steady-state power output of OIHP solar cells based on different HTLs. (d) PCE histogram of 36 solar cell devices each for the QY1-, QY2-, QY3- and Spiro-OMeTAD-modified OIHP films, fitted to a Gaussian distribution (indicated by solid lines).

Table 2 Photovoltaic parameters of OIHP devices based on QY1, QY2, QY3 and Spiro-OMeTAD

Device ID	Scan	J_{sc} (mA cm^{-2})	V_{oc} (V)	FF (%)	PCE (%)	Integrated J_{sc} (mA cm^{-2})
QY1	Reverse	22.54	1.09	73.79	18.23	22.25
QY2	Reverse	22.61	1.10	73.94	18.52	22.37
QY3	Reverse	22.74	1.11	76.29	19.28	22.55
Spiro-OMeTAD	Reverse	22.89	1.10	76.52	19.30	22.64

the fabricated devices are depicted in Fig. 4(b). The integrated J_{sc} of Spiro-OMeTAD, QY1, QY2 and QY3 are found to be 22.64, 22.25, 22.37 and 22.55 mA cm^{-2}, consistent with the J_{sc} values obtained from the *J–V* curves. Maximum power point tracking was performed to evaluate the stable steady-state power output. Biases of 0.87, 0.89, 0.91 and 0.92 V were applied to the QY1-, QY2-, QY3- and Spiro-OMeTAD-based OIHP devices, respectively (Fig. 4(c)). The devices yield stabilized PCEs of 19.22% for the Spiro-OMeTAD and 19.19% for the QY3-modified devices. In order to study the repeatability of the devices, 36 identical devices were prepared for each HTM for statistical efficiency analysis, as shown in Fig. 4(d). The average PCE values of QY1, QY2, QY3 and Spiro-OMeTAD were calculated to be 18.02%, 18.28%, 19.04% and 19.07%, respectively. The chat box of the corresponding J_{sc}, V_{oc} and FF are shown in Fig. S10 (ESI†). The normal distribution of the PCE proved to be the outstanding reproducibility of the manufacturing process. All these results suggest the superior photovoltaic performance of QY3-based OIHP solar cells and the potential of QY3 as an excellent HTM for OIHP solar cells.

3.4 Steady-state and time-resolved photoluminescence and transient photocurrent/photovoltage studies

To understand the underlaying reason behind the enhancement in photovoltaic performance of QY3-HTLs, steady-state PL and TRPL spectra of QY-HTLs prepared on top of perovskite film were carried out, as in Fig. 5(a and b). The lower PL intensity noted for perovskite/QY3 compared to its counterparts implies a more effective charge transfer at the interface of perovskite/QY3. The carrier lifetime lengthening in the QY-HTL was confirmed through TRPL studies, where the average lifetimes of the QY1-, QY2- and QY3-modified perovskite films were 1.72 ns, 1.23 ns and 0.89 ns, respectively. The changes in carrier lifetime are consistent with the tendency of FF and V_{oc} depending on the QY-HTLs. Such lifetime lengthening further confirms that QY3 shows the most effective charge transfer at

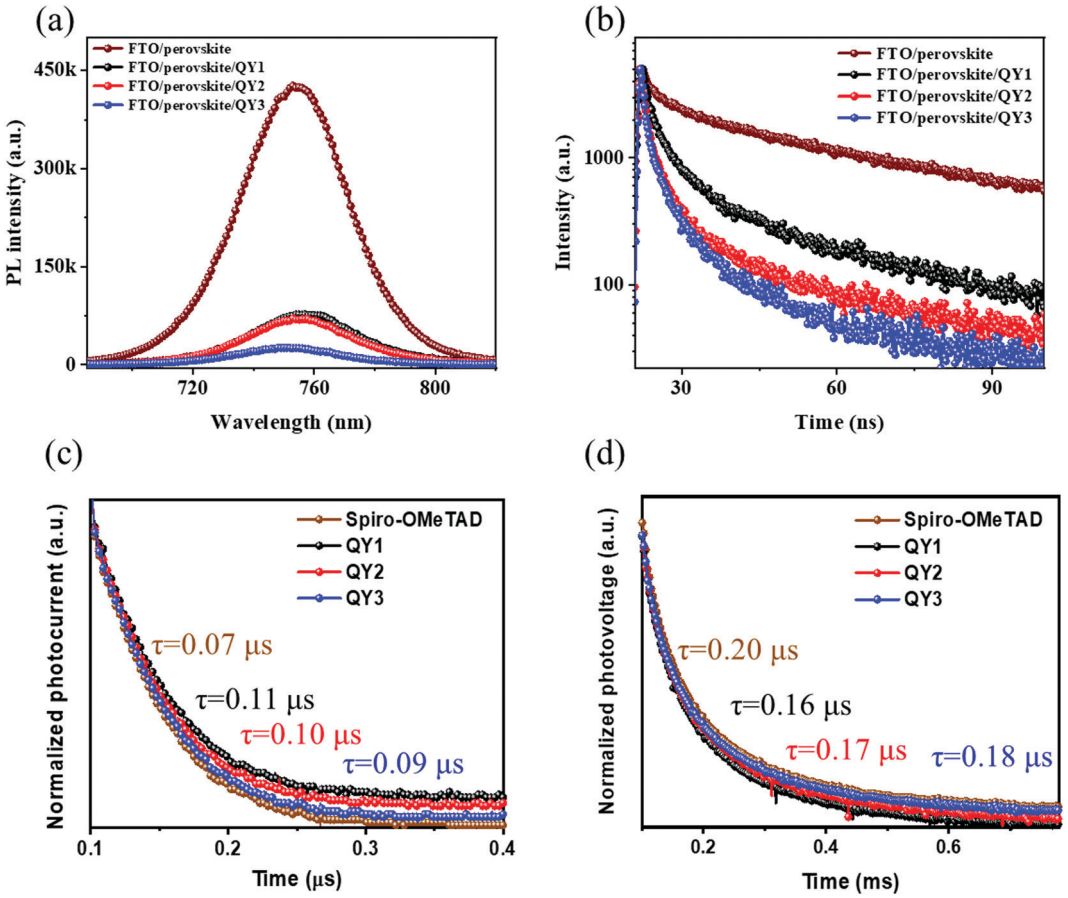

Fig. 5 (a) Steady-state PL spectra and (b) TRPL decay spectra of perovskite film with and without HTLs. (c) Normalized transient photocurrent and (d) transient photovoltage of QY-HTL-based OIHP solar cells.

the interface, which can be explained by the enhanced FF and V_{oc}. Furthermore, the similar PL quenching and carrier lifetime of QY3 and Spiro-OMeTAD indicate that QY3 can extract/transport holes from perovskite film as efficiently as Spiro-OMeTAD. The fitting details and values for the TRPL are summarized in Table S6 (ESI†). To gain insight into the charge carrier dynamics in the QY-HTL-based OIHP solar cells, transient photocurrent (TPC) and transient photovoltage (TPV) decay measurements were performed, as shown in Fig. 5(c and d). The photocurrent decay was measured under the short-circuit condition for the OIHP devices (Fig. 5(c)). In comparison to the decay time of QY1 and QY2, the decay time of QY3 is faster, suggesting better charge carrier extraction capability and reduced extraction time. The TPV measurements were conducted under the open-circuit condition (Fig. 5(d)). A longer photovoltage decay time of QY3 (0.18 μs) was obtained, compared to that for QY1 (0.17 μs) and QY2 (0.16 μs), which is closest to the value of Spiro-OMeTAD (0.20 μs). The longer carrier lifetime can be explained by the QY3-treated devices having fewer non-radiative recombination sites due to suppressed non-radiative recombination at the perovskite/QY3-HTL interface, which further supports the enhancement of FF and V_{oc} in QY3-based OIHP devices.

It can be seen that the performance of the OIHPs is highly dependent on the π-conjugated bridge in the core of the HTMs. Compared to QY1, nearly two orders of magnitude higher hole mobility is achieved from the π-conjugated bridge in the core center *via* incorporation of an S atom. This suggests that simply creating π-conjugation in the core center is an effective approach to improve the hole mobility of HTMs. Based on QY2, we further extended the conjugation length by incorporating thiol groups in the core center for QY3, leading to a higher hole mobility compared to QY2 as a result of more effective intermolecular stacking. Although there is a slight increase in hole mobility for QY3 in experimental results, the result of improving the hole mobility is consistent with previous results, where increasing the π-bridge conjugation length in HTMs enables increase in hole mobility, leading to improved device performance.[23,32–34] In addition, the morphology of QY3 shows a relatively smooth surface roughness (RMS = 10.9 nm) compared with QY1 (RMS = 12.9 nm) and QY2 (RMS = 12.1 nm), implying a superior interfacial contact between the perovskite film and the HTL. The smoother morphology observed is likely to improve the charge extraction and transport. The results of PL, TPV and TPC measurements are consistent with the resulting device performance. Hence, improved hole transferability and extraction efficiency by means of reinforcing the conjugation in the core center can be attributed to the reduction of the non-radiative recombination at the perovskite/HTL interface, leading to the enhancement of *Voc*, *Jsc* and FF.

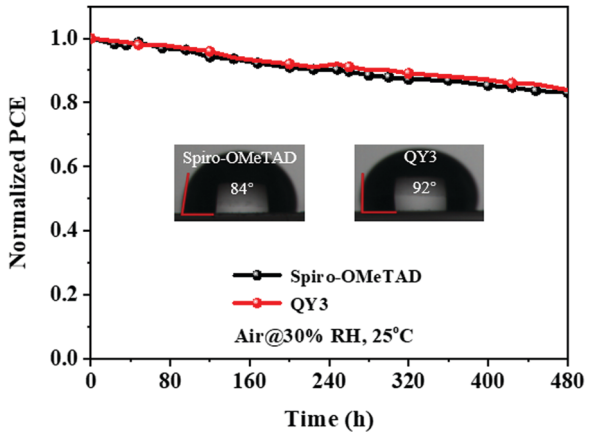

Fig. 6 Stability tests for OIHP solar cells based on QY3 and Spiro-OMeTAD (inset: water contact angle of QY3-HTL and Spiro-OMeTAD).

3.5 Stability studies

It is well known that the HTL plays a critical role in maintaining the stability of OIHP solar cells. Finally, the ambient stabilities of the devices with QY3-HTLs and Spiro-OMeTAD were compared, as shown in Fig. 6. To investigate the effectiveness of the protection capability of QY-HTLs, an ambient stability test of OIHP solar cells was carried out at 25 °C under a relative humidity of ~30% without any encapsulation. As displayed in Fig. 6, the device with QY3 shows better moisture tolerance, retaining 83.95% of its initial PCE on storing for 480 h. The device modified with Spiro-OMeTAD shows a 16.8% reduction in PCE under the same testing conditions, which is comparable with QY3. The water contact angle measurement was conducted to reveal the hydrophobicity of QY3-HTL. Contact angles of 92° and 84° were obtained on films with QY3 and Spiro-OMeTAD, respectively. This indicates that a higher hydrophobicity of the QY3 film is able to prevent interdiffusion of moisture into the perovskite layer as efficiently as Spiro-OMeTAD, and contributes to the decent stability of the QY3-based OIHP solar cells.

4. Conclusions

In summary, we have successfully synthesized three novel D–π–D HTMs incorporating 9*H*-fluorene, dibenzo[*b*,*d*]thiophene and 3,7-di(thiophen-2-yl)dibenzo[*b*,*d*]thiophene through facile and low-cost synthetic routes for OIHP solar cells. The suitable band alignments and high hole mobilities allow effective hole extraction and transportation in OIHP solar cells. The QY3-HTL-based OIHP devices afforded an improved PCE of 19.25% owing to their higher hole mobility and reduced non-radiative recombination at the interface. Our results offer valuable insights into the rational design of D–π–D HTMs for application in highly efficient and stable OIHP solar cells in the future.

Author contributions

Ouyang Mei synthesized the materials and fabricated the solar cells. Tai Wu, Rong Jun Zhao, and Peng Wang carried out the electrical measurements. Yuan Ju Zhao, Gao Yuan Liu, Qian Lai and Li Qiong Zhu carried out material characterization. Lin Xie helped in the discussion of materials, device characterization and wrote the manuscript. Yong Hua designed the materials and supervised the progress of this project.

Conflicts of interest

The authors declare that they have no known competing financial interests or personal relationships that could have appeared to influence the work reported in this paper.

Acknowledgements

L. Xie thanks High-Level Talents of Yunnan University (CZ21623201). Y. Hua thanks National Natural Science Foundation of China (22065038), the Key Project of Natural Science Foundation of Yunnan (KC10110419), High-Level Talents Introduction in Yunnan Province (C619300A010), the Fund for Excellent Young Scholars of Yunnan (K264202006820), the Program for Excellent Young Talents of Yunnan University and Major Science (C176220200), International Joint Research Center for Advanced Energy Materials of Yunnan Province (202003AE140001) and Technology Project of Precious Metal Materials Genetic Engineering in Yunnan Province (No. 2019Z E001-1, 202002AB080001) for financial support.

References

1 N. G. Park, Perovskite solar cells: an emerging photovoltaic technology, *Mater. Today*, 2015, 65–72.
2 B. Li, V. Ferguson, S. R. P. Silva and W. Zhang, Defect engineering toward highly efficient and stable perovskite solar cells, *Adv. Mater. Interfaces*, 2018, **5**, 1–25.
3 K. Hwang, Y.-S. Jung, Y.-J. Heo, F. H. Scholes, S. E. Watkins, J. Subbiah, D. J. Jones, D.-Y. Kim and D. Vak, Toward large scale roll-to-roll production of fully printed perovskite solar cells, *Adv. Mater.*, 2015, **27**, 1241–1247.
4 M. Grätzel, The rise of highly efficient and stable perovskite solar cells, *Acc. Chem. Res.*, 2017, **50**, 487–491.
5 H.-S. Kim, C.-R. Lee, J.-H. Im, K.-B. Lee, T. Moehl, A. Marchioro, S.-J. Moon, R. Humphry-Baker, J.-H. Yum, J. E. Moser, M. Grätzel and N.-G. Park, Lead iodide perovskite sensitized all-solid-state submicron thin film mesoscopic solar cell with efficiency exceeding 9%, *Sci. Rep.*, 2012, **2**, 591.
6 M. Lyu and N.-G. Park, Effect of additives ax (a = fa, ma, cs, rb, nh_4, x = cl, br, i) in $fapbi_3$ on photovoltaic parameters of perovskite solar cells, *Sol. RRL*, 2020, **4**, 2000331.
7 M. Saliba, T. Matsui, J. Y. Seo, K. Domanski, J. P. Correa-Baena, M. K. Nazeeruddin, S. M. Zakeeruddin, W. Tress, A. Abate, A. Hagfeldt and M. Grätzel, Cesium-containing triple cation perovskite solar cells: improved stability, reproducibility and high efficiency, *Energy Environ. Sci.*, 2016, **9**, 1989–1997.

8 L. Xie, H. Hwang, M. Kim and K. Kim, Ternary solvent for $CH_3NH_3PbI_3$ perovskite films with uniform domain size, *Phys. Chem. Chem. Phys.*, 2017, **19**, 1143–1150.
9 M. Kim, G. H. Kim, T. K. Lee, I. W. Choi, H. W. Choi, Y. Jo, Y. J. Yoon, J. W. Kim, J. Lee, D. Huh, H. Lee, S. K. Kwak, J. Y. Kim and D. S. Kim, Methylammonium chloride induces intermediate phase stabilization for efficient perovskite solar cells, *Joule*, 2019, **3**, 2179–2192.
10 V. Blažek Bregović, N. Basarić and K. Mlinarić-Majerski, Anion binding with urea and thiourea derivatives, *Coord. Chem. Rev.*, 2015, **295**, 80–124.
11 L. Gao, G. Wu, J. Ma, T. Jiang, B. Chang, Y. Huang and S. Han, SnO_2 quantum dots@graphene framework as a high-performance flexible anode electrode for lithium-ion batteries, *ACS Appl. Mater. Interfaces*, 2020, **12**, 12982–12989.
12 C. Liu, L. Zhang, Y. Li, X. Zhou, S. She, X. Wang, Y. Tian, A. K. Y. Jen and B. Xu, Highly stable and efficient perovskite solar cells with 22.0% efficiency based on inorganic–organic dopant-free double hole transporting layers, *Adv. Funct. Mater.*, 2020, **1908462**, 1–8.
13 P. K. Kung, M. H. Li, P. Y. Lin, Y. H. Chiang, C. R. Chan, T. F. Guo and P. Chen, A review of inorganic hole transport materials for perovskite solar cells, *Adv. Mater. Interfaces*, 2018, **5**, 1–35.
14 J. Jeong, M. Kim, J. Seo, H. Lu, P. Ahlawat, A. Mishra, Y. Yang, M. A. Hope, F. T. Eickemeyer, M. Kim, Y. J. Yoon, I. W. Choi, B. P. Darwich, S. J. Choi, Y. Jo, J. H. Lee, B. Walker, S. M. Zakeeruddin, L. Emsley, U. Rothlisberger, A. Hagfeldt, D. S. Kim, M. Grätzel and J. Y. Kim, Pseudo-halide anion engineering for α-$FAPbI_3$ perovskite solar cells, *Nature*, 2021, **592**, 381–385.
15 Y. Hua, J. Zhang, B. Xu, P. Liu, M. Cheng, L. Kloo, E. M. J. Johansson, K. Sveinbjörnsson, K. Aitola, G. Boschloo and L. Sun, Facile synthesis of fluorene-based hole transport materials for highly effifcient perovskite solar cells and solid-state dye-sensitized solar cells, *Nano Energy*, 2016, **26**, 108–113.
16 B. Xu, J. Zhang, Y. Hua, P. Liu, L. Wang, C. Ruan, Y. Li, G. Boschloo, E. M. J. Johansson, L. Kloo, A. Hagfeldt, A. K. Y. Jen and L. Sun, Tailor-making low-cost spiro[fluorene-9,9′-xanthene]-based 3d oligomers for perovskite solar cells, *Chem*, 2017, **2**, 676–687.
17 J. H. Heo, S. H. Im, J. H. Noh, T. N. Mandal, C.-S. Lim, J. A. Chang, Y. H. Lee, H. Kim, A. Sarkar, M. K. Nazeeruddin, M. Grätzel and S. Il Seok, Efficient inorganic–organic hybrid heterojunction solar cells containing perovskite compound and polymeric hole conductors, *Nat. Photonics*, 2013, **7**, 486–491.
18 E. H. Jung, N. J. Jeon, E. Y. Park, C. S. Moon, T. J. Shin, T.-Y. Yang, J. H. Noh and J. Seo, Efficient, stable and scalable perovskite solar cells using poly(3-hexylthiophene), *Nature*, 2019, **567**, 511–515.
19 N. Arora, M. I. Dar, A. Hinderhofer, N. Pellet, F. Schreiber, S. M. Zakeeruddin and M. Grätzel, Perovskite solar cells with CuSCN hole extraction layers yield stabilized efficiencies greater than 20%, *Science*, 2017, **358**, 768–771.
20 M. B. Islam, M. Yanagida, Y. Shirai, Y. Nabetani and K. Miyano, Hole transport layer for perovskite solar cells with improved stability and reproducibility, *ACS Omega*, 2017, **2**, 2291–2299.
21 S. Pitchaiya, M. Natarajan, A. Santhanam, V. Asokan, A. Yuvapragasam, V. Madurai Ramakrishnan, S. E. Palanisamy, S. Sundaram and D. Velauthapillai, A review on the classification of organic/inorganic/carbonaceous hole transporting materials for perovskite solar cell application, *Arab. J. Chem.*, 2020, **13**, 2526–2557.
22 S. Paek, I. Zimmermann, P. Gao, P. Gratia, K. Rakstys, G. Grancini, M. K. Nazeeruddin, M. A. Rub, S. A. Kosa, K. A. Alamry and A. M. Asiri, Donor–π–donor type hole transporting materials: marked π-bridge effects on optoelectronic properties, solid-state structure, and perovskite solar cell efficiency, *Chem. Sci.*, 2016, **7**, 6068–6075.
23 Y. Ou, A. Sun, H. Li, T. Wu, D. Zhang and P. Xu, Developing D–π–D hole-transport materials for perovskite solar cells: the effect of the π-bridge on device performance, *Mater. Chem. Front.*, 2021, **5**, 876–884.
24 G. Reddy, P. Basak, L. A. Jones, E. Della Gaspera, N. Islavath and L. Giribabu, Crystalline D–π–D porphyrin molecules as a hole-transporting material for printable perovskite solar cells, *Sol. Energy*, 2020, **206**, 539–547.
25 T. P. I. Saragi, T. Spehr, A. Siebert, T. Fuhrmann-Lieker and J. Salbeck, Spiro compounds for organic optoelectronics, *Chem. Rev.*, 2007, **107**, 1011–1065.
26 A. Batra, G. Kladnik, H. Vázquez, J. S. Meisner, L. Floreano, C. Nuckolls, D. Cvetko, A. Morgante and L. Venkataraman, Quantifying through-space charge transfer dynamics in π-coupled molecular systems, *Nat. Commun.*, 2012, **3**, 1086.
27 D. Zhang, T. Wu, P. Xu, Y. Ou, A. Sun, H. Ma, B. Cui, H. Sun, L. Ding and Y. Hua, Importance of terminated groups in 9,9-bis(4-methoxyphenyl)-substituted fluorene-based hole transport materials for highly efficient organic-inorganic hybrid and all-inorganic perovskite solar cells, *J. Mater. Chem. A*, 2019, **7**, 10319–10324.
28 Y. Tian, L. Tao, C. Chen, C. Wu, H. Lu, X. Yang, H. Li and M. Cheng, Benzo[1,2-*c*:4,5-*c*′]dithiophene-4,8-dione (BDD) core building block based dopant-free hole-transport materials for efficient and stable perovskite solar cell, *ACS Appl. Energy Mater.*, 2020, **3**, 10333–10339.
29 D. Zhu, X. Bao, Q. Zhu, C. Gu, M. Qiu, S. Wen, J. Wang, B. Shahid and R. Yang, Thienothiophene-based copolymers for high-performance solar cells, employing different orientations of the thiazole group as a π bridge, *Energy Environ. Sci.*, 2017, **10**, 614–620.
30 K. W. Lai, C. C. Chang and C. W. Chu, Benzodithiophene-based small molecules with various termini as hole transporting materials in efficient planar perovskite solar cells, *Org. Electron.*, 2021, **89**, 106010.
31 T. Wu, R. Zhuang, R. Zhao, R. Zhao, L. Zhu, G. Liu, R. Wang, K. Zhao and Y. Hua, Understanding the effects of fluorine substitution in lithium salt on photovoltaic properties and

stability of perovskite solar cells, *ACS Energy Lett.*, 2021, **6**, 2218–2228.

32 W. Hu, Z. Zhang, J. Cui, W. Shen, M. Li and R. He, Influence of π-bridge conjugation on the electrochemical properties within hole transporting materials for perovskite solar cells, *Nanoscale*, 2017, **9**, 12916.

33 B. Xu, J. Zhang, Y. Hua, P. Liu, L. Wang, C. Ruan, Y. Li, G. Boschloo, E. M. J. Johansson, L. Kloo, A. Hagfeldt, A. K. Y. Jen and L. Sun, Tailor-making low-cost spiro[fluorene-9,9′-xanthene]-based 3d oligomers for perovskite solar cells, *Chem*, 2017, **2**, 676.

34 J. Terao, A. Wadahama, A. Matono, T. Tada, S. Watanabe, S. Seki, T. Fujihara and Y. Tsuji, Design principle for increasing charge mobility of π-conjugated polymers using regularly localized molecular orbitals, *Nat. Commun.*, 2013, **4**, 1691.

